Dynamic behaviour of polymers at high strain-rates based on split Hopkinson pressure bar tests

Y.B. Lu, Q.M. Li

Accepted Manuscript

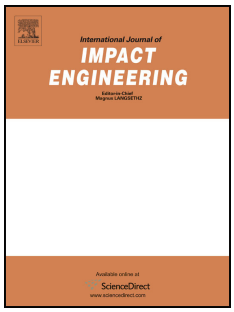

Title: Dynamic behaviour of polymers at high strain-rates based on split Hopkinson pressure bar tests

Authors: Y.B. Lu, Q.M. Li

PII: S0734-743X(10)00122-3

DOI: 10.1016/j.ijimpeng.2010.08.001

Reference: IE 1905

To appear in: *International Journal of Impact Engineering*

Received Date: 4 August 2008

Revised Date: 6 August 2010

Accepted Date: 9 August 2010

Please cite this article as: Lu YB, Li QM. Dynamic behaviour of polymers at high strain-rates based on split Hopkinson pressure bar tests, International Journal of Impact Engineering (2010), doi: 10.1016/j.ijimpeng.2010.08.001

Dynamic behaviour of polymers at high strain-rates based on split Hopkinson pressure bar tests

Y.B.Lu and Q.M.Li*

School of Mechanical, Aerospace and Civil Engineering, Pariser Building,

The University of Manchester, Sackville Street, Manchester M13 9PL, UK

Abstract: Dynamic behaviour of polymers at high strain-rates from 10^1 to 10^4 s^{-1} is frequently investigated by split Hopkinson pressure bar (SHPB) technique. It is found that the apparent strain-rate effect on the dynamic yield stress of polymers based on SHPB tests may include significant contributions from lateral confinement effects when the strain-rate is beyond a transition strain-rate. A methodology based on numerical SHPB tests and the constitutive equation without considering strain-rate effect is proposed to identify this transition strain-rate. Experimentally-measured strain-rate dependence of the peak stress up to the transition strain-rate is recommended for the determination of the strain-rate dependence of the polymer, which is subsequently implemented into a dynamic constitutive equation including strain-rate and temperature effects. This dynamic constitutive equation together with a kinetic friction model is used to simulate the SHPB tests in independent publications. Reasonably good agreements between numerical predictions and experimental results are observed for a range of polymers at strain-rates below 10^4 s^{-1}.

Keywords: polymers, strain-rate effects, split Hopkinson pressure bar, Drucker-Prager model, lateral confinement

* Corresponding author, e-mail: qingming.li@manchester.ac.uk

1. Introduction

Dynamic compression tests based on split Hopkinson pressure bar (SHPB) technique are commonly used to determine the strain-rate dependence of dynamic yield stress for polymers at strain-rates from 10^1 to 10^4 s^{-1}. The dependence of the dynamic flow stress on strain-rate for polymers is normally represented by a dynamic increase factor (DIF) defined by the ratio of the dynamic first peak stress to its quasi-static value in compression in the true uniaxial stress–strain curve, since the peak stress is most easily recognized in the stress–strain curves. It has been shown that the DIFs of polymers increase with strain-rates [e.g. Polymethyl-methacrylate (PMMA) in Chen et al.(2002), polyamide-imide (PAI) in Richeton et al.(2006), Polycarbonate (PC) in Mulliken and Boyce(2006)].

It is expected that a valid SHPB test can give the uniaxial stress–strain curve at the given environmental temperature and strain-rate, which requires uniaxial stress state, stress uniformity and small variations of temperature and strain-rate in the SHPB specimen during the effective testing range. However, these requirements may not be satisfied in some SHPB tests due to non-strain-rate factors [e.g. the adiabatic heating effect in Walley et al.(1989), the wave propagation effect in Dioh et al.(1995)], and therefore, the measured strain-rate effects may not represent the genuine strain-rate dependence of the material. The lateral confinement, which is induced by inertia effects [e.g. Kolsky(1949), Davies and Hunter(1963), Haddow(1965), Samanta(1971), Gorham(1989, 1991), Gorham et al.(1984, 1992), Malinowski and Klepaczko(1986), Lee and Kim(2000), Benaceur et al.(2008)] and interfacial friction effects [e.g. Lindholm(1964), Bowden and Tabor(1973), Bertholf and Karnes(1975), Briscoe and Nosker(1984, 1985), Malinowski and Klepaczko(1986), Walley et al.(1989), Gorham et al.(1992), Gray(2000), Lee and Kim(2000), Hall and Guden(2003), Meng and Li(2003), Trautmann et al.(2005), Hartley et al.(2007)], are the common non-strain-rate factors that may significantly affect SHPB results. Such lateral confinement can lead to significant increase of the axial compressive strength of those engineering materials whose strengths are hydrostatic-pressure-dependent.

For concrete-like materials, it has been shown that there exists a transition strain-rate, beyond which, the lateral confinement effects on the axial strength enhancement increase rapidly with strain-rate [Li and Meng(2003)] due to the transition from a uniaxial stress state at low strain-rates to a multiaxial stress state at high strain-rates. Thus, the observed rapid increase of DIF of concrete-like materials beyond this transition strain-rate is mainly due to lateral confinement effects rather than genuine strain-rate effects. The importance of this transition strain-rate, which has been ignored generally in the interpretation of SHPB results in many publications on SHPB tests of both concrete-like and polymeric materials, was addressed in a review article on experimental techniques for high strain-rate deformation [Field et al.(2004)]. It is anticipated that similar transition strain-rate exists in the dynamic compressive tests of all hydrostatic-pressure-sensitive materials including polymers [Bardia and Narasimhan(2006)], which motivates this research. Actually, such transition strain-rate has been shown for polymers [e.g. in Chou et al.(1973), Rietsch and Bouette(1990) and Dioh et al.(1993) for PC], which, however, were interpreted as the start of significant strain-rate dependence of the tested polymers. In a one-dimensional numerical simulation of SHPB tests on polymeric specimens based on an elastic-plastic model with strain-rate dependence described by Eyring model [Eyring(1936)], Zhao(1998) showed that the thickness of the SHPB specimen does not influence the axial stress equilibrium in the specimen, but may introduce three-dimensional effects from radial inertia and interfacial friction in SHPB tests. For hydrostatic-pressure-sensitive materials, this issue should be seriously investigated.

A research methodology is described in Section 2 for the determination of the transition strain-rate. A method is proposed in Section 3 to determine the real strain-rate effect, which is implemented in a phenomenological dynamic constitutive model. Numerical predictions of SHPB results and DIFs are presented and compared with a range of SHPB experimental results on PC specimens in Section 4. Conclusions are made in Section 5.

2. Methodology and Quasi-Static Material Model

We employed a 'reconstitution method' and numerical SHPB simulations to find the transition strain-rate when the material is described as a strain-rate-independent model based on its quasi-static constitutive equation [Li and Meng(2003)]. All important factors except strain-rate and temperature are considered in the numerical SHPB simulation. Since the quasi-static constitutive equation does not include strain-rate and temperature effects, any discrepancies between the input stress–strain curve and the reconstituted apparent stress–strain curve are due to other non-strain-rate causes. The details of quasi-static constitutive equation of polymer (PC is used as an example in this study) will be discussed in Section 2.2. Numerical SHPB model will be shown in Section 2.3. The determination of the transition strain-rate is presented in Section 2.4. It will be shown that a distinct transition strain-rate representing the fundamental change from a uniaxial stress state to a multiaxial stress state can be identified from DIF curve determined by above methodology.

After the transition strain-rate is identified, a method is proposed in Section 3 to determine the real strain-rate effect, which is then used to determine the strain-rate dependence in a phenomenological dynamic constitutive equation. Finally, the dynamic constitutive equation is used in numerical SHPB models to predict the responses of the SHPB specimen, which are compared with independent SHPB experimental data to show the validity of the methodology.

The SHPB pressure bars and the specimen are simulated as a structural problem to obtain the reconstituted stresses and strains based on the modified three-wave formulae [Song and Hu(2005)],

$$\sigma_z(t) = \frac{A_b E_b \varepsilon_t(t)}{A_s}, \tag{1a}$$

$$\dot{\varepsilon}_z(t) = \frac{c_b}{L_s}[\varepsilon_i(t) - \varepsilon_r(t) - \varepsilon_t(t)], \tag{1b}$$

$$\varepsilon_z(t)=\frac{c_b}{L_s}\int_0^t[\varepsilon_i(t)-\varepsilon_r(t)-\varepsilon_t(t)]dt. \quad (1c)$$

where $\sigma_z(t)$, $\dot{\varepsilon}_z(t)$ and $\varepsilon_z(t)$ are engineering stress, strain-rate and strain; A_b, E_b and c_b ($c_b=\sqrt{E_b/\rho_b}$ with ρ_b being the density of the pressure bar material) are the cross-sectional area, Young's modulus and the elastic wave speed of the pressure bars, respectively; L_s is the original length of the specimen and $A_s=\pi d_0^2/4$ is the original cross-sectional area of the specimen with d_0 being the original diameter of the SHPB specimen; $\varepsilon_i(t)$ and $\varepsilon_r(t)$ are the incident and reflected axial strains on the incident pressure bar, respectively, and $\varepsilon_t(t)$ is the transmitted axial strain on the transmission pressure bar. For the valid application of Eqs.(1a-c), the equilibrium equation $P_1=P_2$ or $\varepsilon_i+\varepsilon_r=\varepsilon_t$ should be approximately satisfied to achieve the stress homogeneity in SHPB specimen, where P_1 and P_2 are the forces acting on the two interfaces between the specimen and the incident and transmission pressure bars.

As polymers may experience large deformation, it is necessary to convert engineering axial stress σ_z, strain-rate $\dot{\varepsilon}_z$ and strain ε_z to true axial stress $\sigma_z^T(t)$, strain-rate $\dot{\varepsilon}_z^T(t)$ and strain $\varepsilon_z^T(t)$ using following equations [e.g. Frew et al.(2005), Arriaga et al.(2007)]

$$\sigma_z^T(t)=\sigma_z(t)[1-\varepsilon_z(t)], \quad (2a)$$

$$\dot{\varepsilon}_z^T(t)=\frac{\dot{\varepsilon}_z(t)}{1-\varepsilon_z(t)}, \quad (2b)$$

$$\varepsilon_z^T(t)=-\ln[1-\varepsilon_z(t)]. \quad (2c)$$

Equation (2a) is based on plastic incompressibility (or constancy of volume) during plastic deformation of the material. The incompressibility of PC can be approximately satisfied when the strain is greater than the yield strain [e.g. Brady and Yeh(1971), Pampillo and Davis(1971), Wang et al.(1982), Siviour et al.(2005)], therefore, we judged that the use of

Eq.(2a) to convert the engineering stress to true stress for PC is acceptable although its suitability for other polymers needs to be further checked.

2.2 Constitutive equation of polymers

We will focus our investigations on PC because it has been the subject of several high strain-rate deformation studies and a number of SHPB testing data have been compiled for PC. However, the conclusions obtained in this study are expected to be applicable to other conventional SHPB configurations and similar type of polymers.

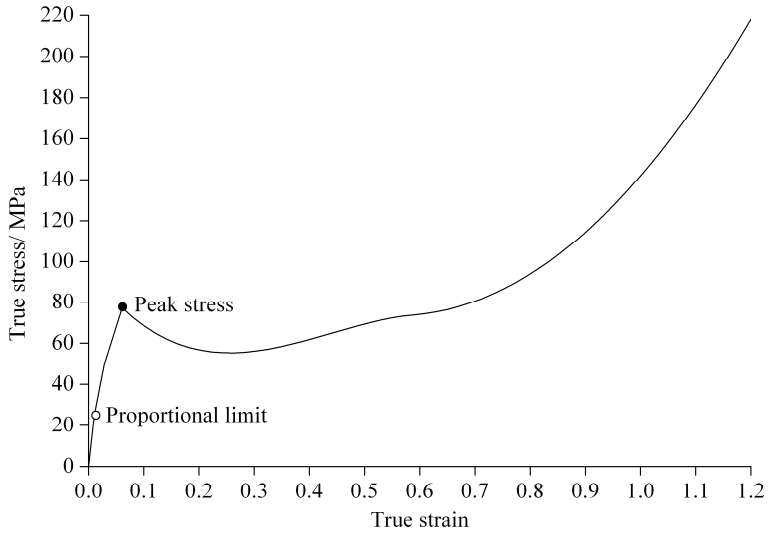

Fig.1. Quasi-static uniaxial compressive true stress–strain curve of PC [Richeton et al.(2006)].

A typical quasi-static true stress–strain relation of PC under uniaxial compression is shown in Fig.1, which usually consists of five regimes, viz. linearly elastic, nonlinearly elastic, yielding, strain-softening and non-linear strain hardening [Chen and Zhang(1997)]. The first regime is up to the proportional limit (σ_y), which is used to determine Young's modulus (E_s), and the second portion is up to the peak stress (σ_p) with corresponding true

strain (ε_p). It should be clarified here that there are different definitions of yield stress. For example, Li and Lambros(2001) defined the yield stress as the first deviation from a linear material response, which is the same as the proportional limit in Fig.1. Other researchers like Trautmann et al.(2005), Siviour et al.(2005) and Richeton et al.(2006) used the first peak stress in the stress–strain curve as the yield stress. It is calculated from Li and Lambros(2001) that the yield stress is about 1/3 of the peak stress, which is supported by the data in Richeton et al.(2006), as shown in Tab.1 in this study. In a numerical model, unless a non-linear elastic model is available, it is convenient to use the proportional limit as the yield stress and treat the non-linear elastic portion in a plastic model, which will be adopted in the present study for the convenience of using ABAQUS code. The dependence of the yield stress on strain-rate is assumed to be identical to that of the peak stress on strain-rate, which is supported by the calculated results of the strain-rate effect defined by DIF using peak stress and the results using yield stress from the experimental data in Li and Lambros(2001). This is understandable because unloading is unlikely during the effective loading duration in an SHPB test.

Experimental evidence suggests that the yielding behavior of polymeric materials is markedly different from that of most metals. In particular, the yield stress under uniaxial tension for a polymer is different from that in uniaxial compression due to the effect of the hydrostatic pressure. Such behavior can be explained by a pressure-dependent yield criterion, such as the Drucker-Prager, Mohr-Coulomb or modified Tresca criteria [Bowden and Jukes(1972)]. A further examination shows that the modified Tresca criterion is unable to predict the behavior of polymers under most conditions [Young and Lovell(1991)] and the Mohr-Coulomb model cannot consider the dependence of failure on the intermediate principal stress. Drucker-Prager model does not have these defects and is more convenient for numerical implementations since it has a continuously varying normal. The extended linear Drucker-Prager model available in ABAQUS, which includes the influence of stress invariants on the loading surface and the plastic deformation of the material, has been

successfully used for a wide range of polymers [e.g. Chowdhury and Narasimhan(2000), Rittel and Brill(2008), Rittel and Dorogoy(2008), Chowdhury et al.(2008)]. We will use the extended linear Drucker-Prager model as the quasi-static constitutive equation for PC.

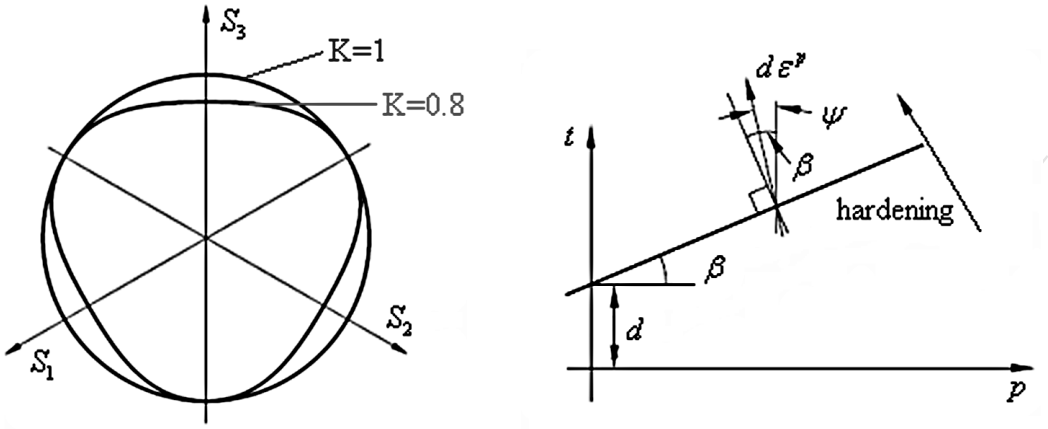

(a) (b)

Fig.2. (a) Typical yield surface of the extended linear Drucker-Prager model in the deviatoric plane, where S_1, S_2 and S_3 are deviatoric stresses; (b) yield surface and flow direction in the *t*-*p* plane [ABAQUS(2007)].

The yield function in the extended linear Drucker-Prager model is given by [ABAQUS(2007)]

$$F = t - p\tan\beta - d = 0 \tag{3}$$

where t is a pseudo-effective stress defined by $t = \frac{q}{2}\left[1+\frac{1}{K}-\left(1-\frac{1}{K}\right)\left(\frac{r}{q}\right)^3\right]$; $q = \sqrt{3J_2}$ and $r^3 = \frac{27}{2}J_3$ with J_2 and J_3 being the second and third invariants of the deviatoric part of the Cauchy stress; $p = -I_1/3$ is the hydrostatic pressure with I_1 being the first stress invariant; β is the slope of the linear yield surface in the *t*-*p* stress plane; $d = \left(1-\frac{1}{3}\tan\beta\right)\sigma_y$ is the static cohesion of the material if hardening is defined by σ_y. K is the ratio between tensile

and compressive triaxial strengths, and thus, controls the dependence of the yield surface on the value of the third invariant J_3, which must be greater than 0.778 [ABAQUS(2007)] to ensure the convexity of the yield surface. The locus of the yield surface will not be circular in the deviatoric stress space if K does not have a value of 1.0 [Fig.2(a)].

The flow potential used in the extended linear Drucker-Prager model is [ABAQUS(2007)]

$$G = t - p\tan\psi, \qquad (4)$$

in which ψ is the dilation angle in the *t*-*p* plane. A geometric interpretation of ψ is shown in Fig.2(b). By comparing Eq.(3) with Eq.(4), it can be seen that $\psi = \beta$ and $\psi \neq \beta$ correspond to associated and non-associated plastic flows, respectively. In particular, $\psi = 0^o$ results in non-dilational plastic flow. More details for the characterization of those parameters in the extended linear Drucker-Prager model can be found in ABAQUS(2007).

Tab.1 Material parameters of pressure bars and PC sample

Material	E (GPa)	ρ (kgm^{-3})	ν	σ_y (MPa)	ε_y	σ_p (MPa)	Drucker-Prager model parameters		
							β (^{o})	ψ (^{o})	K
C350 maraging steel	210	7850	0.35						
	Chen & Luo(2004)		LIGO note(2005)						
PC	2.4	1200	0.38	24.0	0.01	77	15	15	1
	Siviour et al. (2005)		Mulliken & Boyce(2006)	Richeton et al.(2006)					

Based on different experimental techniques, the value of β is reported to be around 15^o for PC [Raghava et al.(1973), Carapellucci and Yee(1983), Quinson et al.(1997), Haufe et al.(2005), Rittel and Dorogoy(2008)], which will be used in the present study. On the other hand, there is a general scarcity of data in literatures regarding appropriate values of ψ for polymers. However, it is observed that ψ mainly influences the post-yield behavior of polymers based on parametric analysis in numerical SHPB tests, and thus, the dependence of DIF on ψ (in the range of 0 to β) in an SHPB test is almost negligible. Therefore, the

associate plastic flow (i.e. $\psi = \beta$ =15°) is assumed in this study. Since there is no available data to fit the parameter *K* and it is found in numerical SHPB tests that the change of *K* from 0.78 to 1 has little influence on the yield stress, *K*=1 is taken in this study. The material parameters used in the extended linear Drucker-Prager model for PC are summarized in Tab.1.

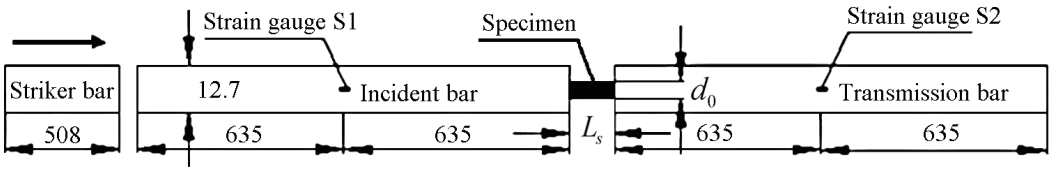

Fig.3. Configuration of the SHPB set-up for numerical simulation, the unit is mm.

2.3 Numerical SHPB model

The whole SHPB set-up as illustrated in Fig.3 is modeled where the dimensions of the SHPB set-up are similar to those used by Richeton et al.(2006) for comparison purpose. PC specimens with various lengths (L_s) of 2.54 mm (with a slenderness ratio $\lambda_s = L_s / d_0$ =0.4), 3.18 mm (λ_s=0.5) and 8 mm (λ_s=1.26) at a fixed diameter of 6.35 mm and various diameters (d_0) of 8 mm (λ_s=0.5), 5.33 mm (λ_s=0.75) and 4 mm (λ_s=1.0) at a fixed length of 4 mm are used in the simulation in order to show the influence of diameter and length (or the slenderness ratio) on the numerical SHPB results.

The pressure bars and specimen of the numerical SHPB employed in the present study are C350 maraging steel and PC, respectively, which are the same as those used in Richeton et al.(2006). However, Richeton et al.(2006) did not give the properties of these materials. The properties of the C350 maraging steel in Tab.1 are taken from Chen and Luo(2004) and LIGO note(2005). The values of Young's modulus and density of PC specimen shown in Tab.1 are referred to Siviour et al.(2005), who used a similar grade of PC to that used in

Richeton et al.(2006). These values are very close to those cited in other references [see e.g. Chowdhury et al.(2008), Rittel and Dorogoy(2008)]. The value of the Poisson's ratio adopted in this paper is from Mulliken and Boyce(2006), who used the same brand of PC as that in Richeton et al.(2006). However, it should be noted that the reported Poisson's ratio values for PC vary between 0.37 [Rittel and Dorogoy(2008)] and 0.40 [Siviour et al.(2005)]. In this study, we use a middle value of 0.38 reported in Mulliken and Boyce(2006). The proportional limit, peak stress and true strain corresponding to the peak stress are taken from the quasi-static experimental curve presented in Richeton et al.(2006).

Finite element models have been used to simulate the SHPB system including the dynamic deformation of the SHPB specimen, e.g. implicit code FORGE2 [Gavrus et al.(2003)], explicit code RADIOSS [Gavrus et al.(2000)] and ABAQUS [Zencker and Clos(1999), Li and Meng(2003)]. In the present numerical simulation, ABAQUS/Explicit version 6.7-1 with element type CAX4R (axi-symmetric element, reduced integration) is applied. A three-dimensional (3D) model with element type C3D8R (8-node linear brick, reduced integration, hourglass control) is also applied in trial numerical simulations under comparable conditions. It is found that differences between the 3D model results and axi-symmetric model results can be ignored. To save the computation time, axi-symmetric model with CAX4R elements is used in this study. The specimen is meshed into 20 elements in the radial direction and 22 elements in the axial direction. Each elastic pressure bar is represented by 20 elements in the radial direction and 1736 elements in the axial direction with finer meshes near the bar/specimen interfaces, as shown in Fig.4 for only a part of the pressure bars. Mesh dependence analyses have been conducted to compare the current mesh with finer meshes and results based on them have negligible differences. An automatic time-integration scheme offered by ABAQUS/Explicit is used throughout the simulation. For the case shown in Fig.4, the maximum wave frequency is about 1.9 MHz. The sliding is permitted between the specimen and the pressure bar. Friction between the specimen and the pressure bars is ignored initially in order to indentify the transition strain-rate associated with

the inertia-induced lateral confinement. The influence of friction model on the SHPB testing results will be briefly discussed at the end of Section 2.4.

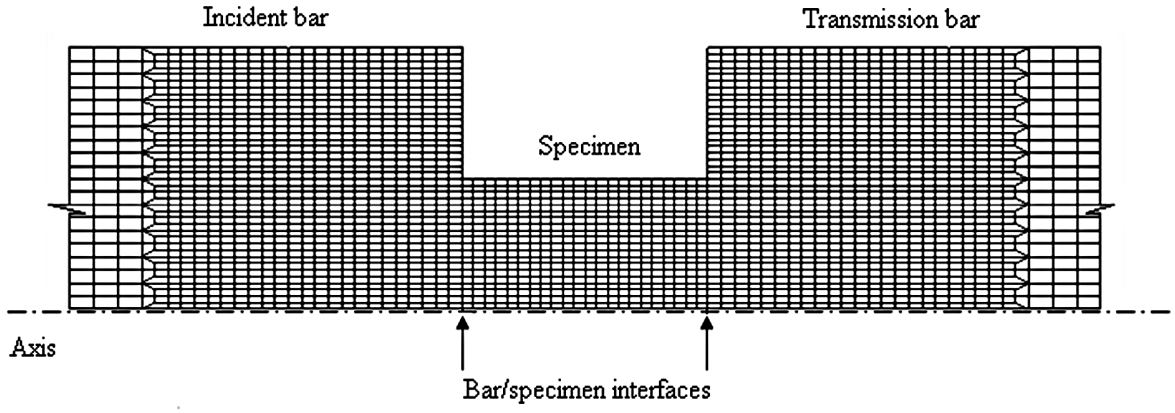

Fig.4. A part of axi-symmetric finite element model of the specimen and pressure bars.

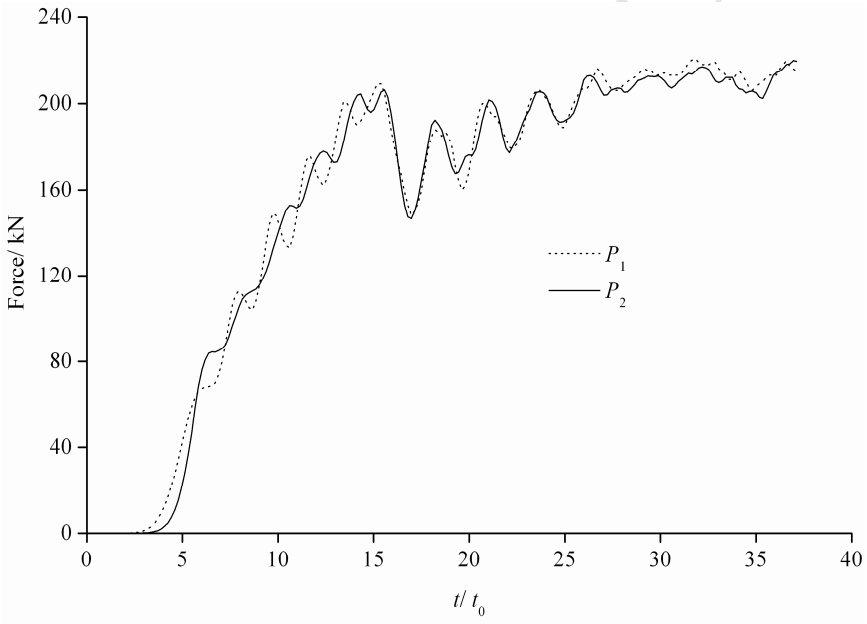

Fig.5. Force histories of $P_1(t)$ and $P_2(t)$ for a PC specimen based on a typical numerical SHPB test, where t/t_0 is the dimensionless time with $t_0 = L_s / c_s = 5.66$ μs for the PC specimen under investigation.

2.4 Determination of the transition strain-rate

Figure 5 gives typical numerical interface force histories of a PC specimen with $L_s = 8$ mm and $d_0 = 6.35$ mm ($\lambda_s = 1.26$), the friction coefficient of zero and the impact velocity of 12 m/s to examine the dynamic stress equilibrium condition within the specimen. These forces are obtained by the summation of the contact force over nodes on the interfaces between the pressure bars and the specimen. It can be seen that homogeneity in the SHPB specimen is achieved after a short time, and thus, using Eqs.(1a-c) for the calculation of the engineering stress, strain-rate and strain in the SHPB specimen is justified.

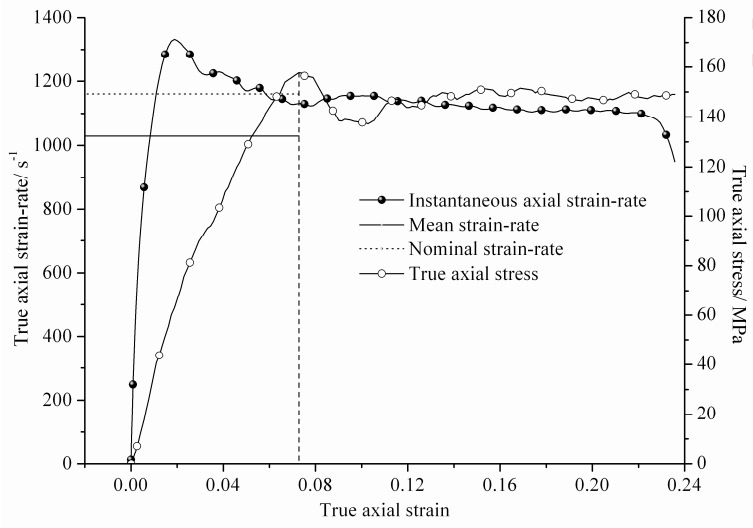

Fig.6. Variations of true axial strain-rate and true axial stress with true axial strain for PC specimens from a typical numerical SHPB test.

The variation of true axial strain-rate with true axial strain for the same PC specimen obtained from the numerical SHPB set-up in Fig.3 at the impact velocity of 12 m/s is shown in Fig.6. It shows that the true axial strain-rate during effective loading period cannot be treated as a constant. The gradient of the true axial strain-rate curve in Fig.6, i.e. the axial strain acceleration, varies with the true axial strain. Since the DIF measured in each SHPB test is associated with a representative strain-rate, it is necessary to give a clear definition of such representative strain-rate used in SHPB tests. Usually, there are three definitions for

such representative strain-rate, viz. mean strain-rate defined as the mean value of the instantaneous axial strain-rate over the loading period [e.g. Grote et al.(2001)]; nominal strain-rate calculated by $\dot{\varepsilon}_n = \varepsilon_z^T(T_d)/T_d$ where $T_d = 2L_{sb}/c_b$ is the wave duration, ε_z^T is true axial strain and L_{sb} is the length of the striker bar [e.g. Hasegawa and Okazaki(1999)]; the true axial strain-rate corresponding to the peak stress [e.g. Gary and Bailly(1998), Zhang et al.(2009)]. As shown in Fig.6, three definitions of the representative strain-rate have different values. However, nearly linear correlations among the true axial strain-rate at the peak stress, mean strain-rate and nominal strain-rate are revealed for all SHPB tests in the present study (Fig.7). The true axial strain-rate corresponding to the peak stress will be used as the representative strain-rate in SHPB tests in the following study.

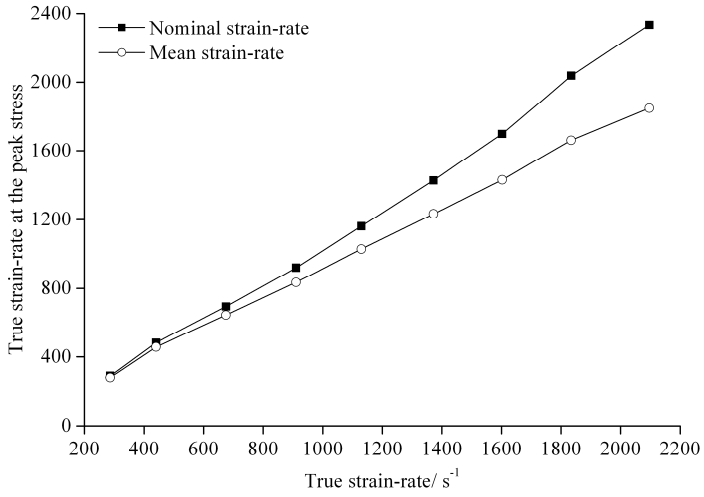

Fig.7. Correlation between the true axial strain-rate at the peak stress and the representative strain-rate defined by other ways for numerical SHPB tests on PC specimens.

For numerical SHPB tests on PC specimens with L_s =8 mm and d_0 =6.35 mm, the reconstituted true axial stress–strain curves and the average hydrostatic pressure, which is obtained by spatially averaging the hydrostatic pressure over the entire specimen elements, versus true axial strain at two different true axial strain-rates of 30 and 1130 s^{-1} are shown in

Fig.8. It shows that the reconstituted true axial stress–strain curve at the true axial strain-rate of 30 s^{-1} in Fig.8(a) fits the input true axial stress–strain curve well, especially before the peak stress is reached. No apparent strain-rate effect is observed and the corresponding hydrostatic pressure keeps about 1/3 of the true axial stress. It transpires that other two principal stresses are both zero at the true axial strain-rate of 30 s^{-1} and the testing sample in this numerical SHPB test is in a uniaxial stress state. In the numerical SHPB tests at other low strain-rates, the inertia-induced lateral confinement is all found to be insignificant and thus the apparent strain-rate effects are not obvious. With the increase of the true axial strain-rate, the yield stress increases dramatically [Fig.8(b)], which are usually attributed to the strain-rate effect in actual SHPB tests. However, as the constitutive model used in the numerical simulations of the SHPB tests is strain-rate-independent, the observed apparent strain-rate effects are not authentic, but due to other causes.

When the average hydrostatic pressures in the specimen at high strain-rates are examined, their values are greater than 1/3 of the corresponding true axial stresses [e.g. Fig.8(b)], which means that the other two principal stresses are not zero. In both the low and high strain-rate cases, the spatial distributions of the hydrostatic pressure are quite uniform around the peak point of the true axial stress because stress waves have reflected more than 10 times in the SHPB specimen, as shown in Fig.5. According to Fig.8, the variation of the average hydrostatic pressure after the peak stress is relatively small.

It is also observed that the hydrostatic pressure in the majority of the SHPB specimen has a relatively homogenous spatial distribution, with highest value at the centre of the specimen and lower value near the side surface, when the overall strain in the specimen is around the true strain corresponding to the peak stress. According to the Drucker-Prager model, the axial compressive strength increases with the hydrostatic pressure. Therefore, the apparent increase of yield stress with strain-rate is not genuine, but caused by the lateral confinement in SHPB tests. Furthermore, the apparent increase of Young's modulus is observed in these simulations, which hints that the discussion about the dependence of Young's modulus on

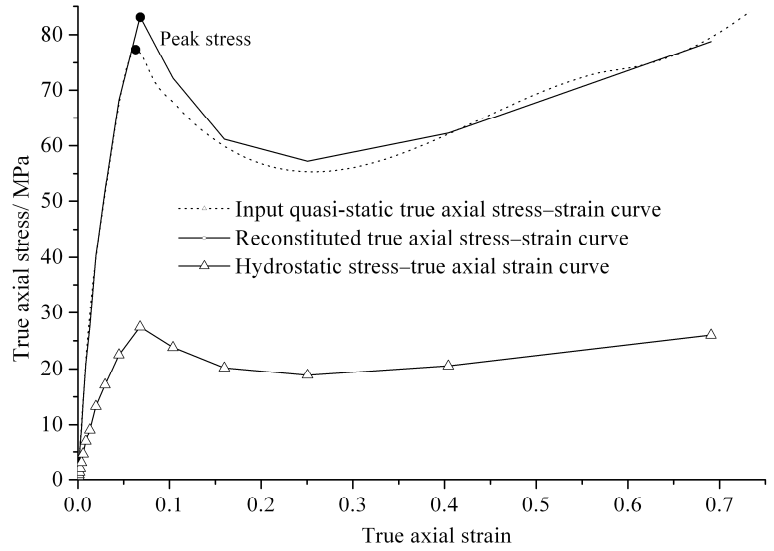

(a)

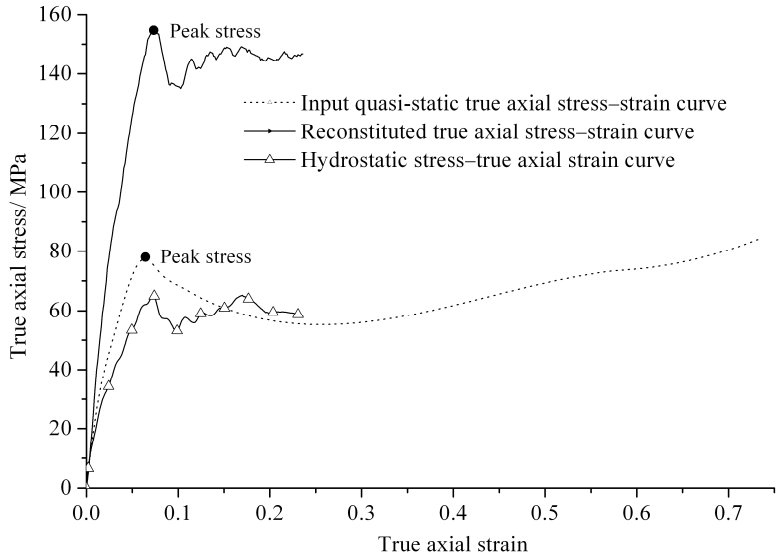

(b)

Fig.8. The true axial stress-strain curve and the average hydrostatic pressure against true axial strain for PC specimens obtained from numerical SHPB tests at a true axial strain-rate of (a) 30 s^{-1}, and (b) 1130 s^{-1}.

The pseudo strain-rate effect on the DIF of PC is simulated and presented in Fig.9 for

specimens with various slenderness ratios, where both the length and diameter of the specimen are varied, to examine the influence of specimen dimensions on the DIF. It is observed that the apparent DIF is indeed insensitive to the slenderness ratio of the specimens in the range of $0.4 \le \lambda_s \le 1.26$. For comparison purpose, SHPB results from independent publications [Li and Lambros(2001), Blumenthal et al.(2002), Siviour et al.(2005), Mulliken and Boyce(2006), Richeton et al.(2006)] are also presented in Fig.9. Although there is a general scarcity of reliable experimental DIF data at strain-rates between 10^1 and 10^2 s^{-1}, a distinct transition strain-rate $\dot{\varepsilon}_t$ can be clearly identified. When $\dot{\varepsilon}_z^T < \dot{\varepsilon}_t$, the numerically-predicted DIF is smaller than the measured DIF while opposite observation is obtained when $\dot{\varepsilon}_z^T > \dot{\varepsilon}_t$. These observations imply that strain-rate effect on the DIF of polymers does exist, which can be estimated based on the true axial stress–strain data before $\dot{\varepsilon}_t$ (as described in Section 3). The SHPB measurements beyond $\dot{\varepsilon}_t$ are influenced by the strain-rate effect, significantly-increased lateral confinement and increased thermal effect (this explains why the predicted DIF is greater than the experimental DIF in Fig.9). Rittel and Brill(2008) reported experiments for cylindrical PMMA specimens confined by tightly-fit metal sleeves and subjected to compression. It is shown that yield stress of PMMA increases with the lateral confinement. However, the apparent dynamic yield stress from SHPB tests on unconfined specimens was treated as uniaxial yield stress [i.e. Eq.(2) in Rittel and Brill(2008)], which may need to be re-examined when $\dot{\varepsilon}_z^T > \dot{\varepsilon}_t$.

Effects of interface friction on the SHPB results have been studied by using the constant friction model [e.g. Bertholf and Karnes(1975), Meng and Li(2003)] and the kinetic friction model [Li et al.(2009)] based on case studies in numerical SHPB tests. It is found that the selection of friction models has negligible influence on $\dot{\varepsilon}_t$. However, the kinetic friction model may influence the numerical simulations when $\dot{\varepsilon}_z^T > \dot{\varepsilon}_t$, and therefore, it will be

included in the numerical SHPB simulations in Section 3. The influence of interface friction on SHPB test results has been studied in detail in Li et al.(2009).

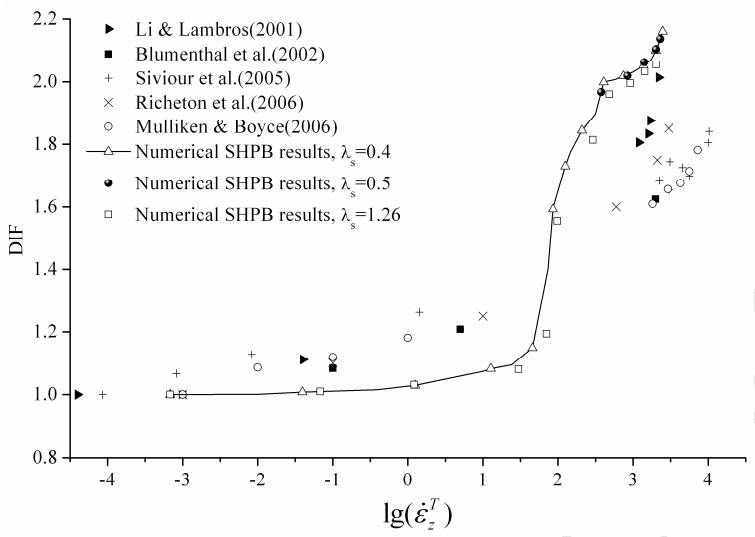

(a)

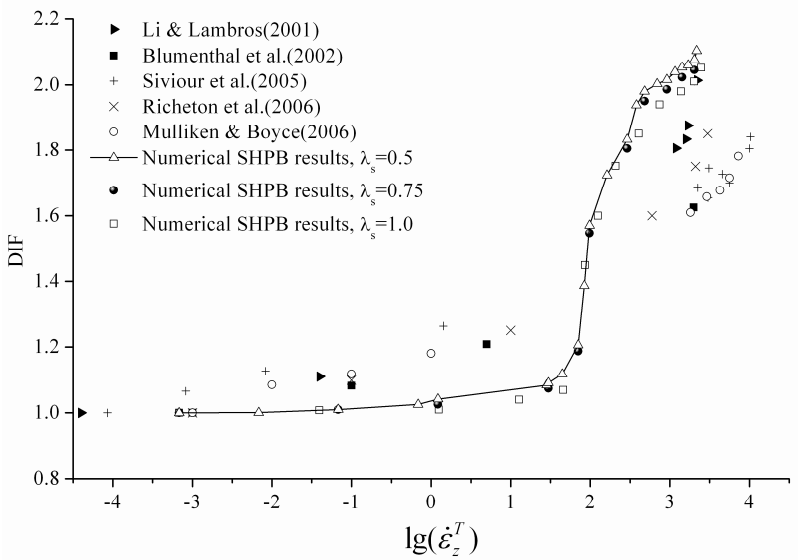

(b)

Fig.9. Comparison between the predicted DIF values for PC specimens with various slenderness ratios λ_s and the measured DIF values from SHPB tests, where d_0 is fixed to be 6.35 mm for case (a) and L_s is fixed to be 4 mm for case (b).

3. Strain-Rate Sensitive Model

The objective of this study is not to propose a new constitutive model for polymers, but to reassess the strain-rate effects for polymeric materials determined by SHPB tests. Although there are some more physics-based polymer models [e.g. Richeton et al.(2005, 2007), Gueguen et al.(2008), Mulliken and Boyce(2006)], we will select a phenomenological constitutive model [Duan et al.(2001, 2003), Yin and Wang(2008)], which is based on the same quasi-static linear Drucker-Prager model used in Section 2 and whose parameters can be easily determined. This selection, however, does not exclude the use of other dynamic constitutive models if they are judged to be more suitable.

When the static material cohesion (d) in Eq.(3) is replaced by the dynamic term (d_D) in Duan et al.(2001, 2003), the extended linear Drucker-Prager model is given by

$$F = t - p\tan\beta - d_D = 0, \tag{5a}$$

$$d_D = K_0 g(\dot{\bar{\varepsilon}}, T)\left\{ f(\bar{\varepsilon}) + \exp(-7\bar{\varepsilon})\left[\frac{\bar{\varepsilon}}{\varepsilon_y}\exp\left(1-\frac{\bar{\varepsilon}}{\varepsilon_y}\right) - f(\bar{\varepsilon}) \right] \right\} \tag{5b}$$

where $\bar{\varepsilon} = \sqrt{\frac{2}{3}(e_{ij}\cdot e_{ij})}$, e_{ij}, $\dot{\bar{\varepsilon}} = \frac{d\bar{\varepsilon}}{dt}$ and T are equivalent plastic strain, deviatoric plastic strain, equivalent plastic strain-rate and absolute temperature (with unit in K), respectively; $f(\bar{\varepsilon}) = [\exp(-K_1\bar{\varepsilon}) + K_2\exp(-K_3\bar{\varepsilon}) + K_4][(1-\exp(-K_5\bar{\varepsilon})]$ is taken to represent strain softening and strain hardening; $g\left(\dot{\bar{\varepsilon}}, T\right) = \exp\left(K_7 \frac{T_0}{T} \right)\left(\frac{\dot{\bar{\varepsilon}}}{\dot{\bar{\varepsilon}}_r} \right)^{K_6}$ with $\dot{\bar{\varepsilon}}_r = 1\,\mathrm{s}^{-1}$ and $T_0 = 273\,\mathrm{K}$ as a reference strain-rate and reference temperature, respectively; $K_0 \sim K_7$ are material coefficients to be determined.

Uniaxial compression tests are frequently used to determine material constants in dynamic constitutive equations of polymers. Based on Eq.(5), the uniaxial dynamic flow

stress (σ_f) in compression is

$$\sigma_f = \frac{K_0}{1-\frac{1}{3}\tan\beta} g(\dot{\varepsilon}_z^T, T)\left\{ f(\varepsilon_z^T) + \exp(-7\varepsilon_z^T)\left[\frac{\varepsilon_z^T}{\varepsilon_y}\exp\left(1-\frac{\varepsilon_z^T}{\varepsilon_y}\right) - f(\varepsilon_z^T)\right]\right\} \tag{6}$$

in which ε_z^T and $\dot{\varepsilon}_z^T$ are true axial strain and strain-rate, respectively.

According to Duan et al.(2001), when the true axial strain reaches the compressive yield strain ε_y, the uniaxial dynamic yield stress in compression σ_{dy} can be expressed as

$$\sigma_{dy} = \frac{K_0}{1-\frac{1}{3}\tan\beta}\exp\left(K_7\frac{T_0}{T}\right)\left(\frac{\dot{\varepsilon}_z^T}{\dot{\varepsilon}_r}\right)^{K_6}\left\{ f(\varepsilon_y) + \exp(-7\varepsilon_y)\left[1-f(\varepsilon_y)\right]\right\} \tag{7}$$

where $\dot{\varepsilon}_r$ =1 s^{-1} is the reference strain-rate. The ratio between two dynamic yield stresses (σ_{dy1} and σ_{dy2}) and their corresponding true axial strain-rates ($\dot{\varepsilon}_{z1}^T$ and $\dot{\varepsilon}_{z2}^T$) have following relationship,

$$\frac{\sigma_{dy2}}{\sigma_{dy1}} = \left(\frac{\dot{\varepsilon}_{z2}^T}{\dot{\varepsilon}_{z1}^T}\right)^{K_6}, \tag{8}$$

which can be used to determine parameter K_6. According to Eq.(8), the value of K_6 is obtained from

$$K_6 = \frac{\lg\left(\sigma_{dy2}/\sigma_{dy1}\right)}{\lg\left(\dot{\varepsilon}_{z2}^T/\dot{\varepsilon}_{z1}^T\right)}. \tag{9}$$

It should be noted that, when selecting the values of yield stresses at different true axial strain-rates, the uniaxial stress state must be guaranteed. Therefore, $\dot{\varepsilon}_{z1}^T$ and $\dot{\varepsilon}_{z2}^T$ must be smaller than the transition strain-rate in Fig.9. Otherwise uniaxial stress state is violated due to the significant influence from the lateral confinement effect discussed in Section 2.4. However, as depicted in Fig.9, there is a general scarcity of experimental DIF data at strain-rates between 10^1 and 10^2 s^{-1}, which results in difficulties in determining the transition

strain-rate accurately. Therefore, in this paper, we took the true axial strain-rate of 10^{-3} s^{-1} as the first point (e.g. $\dot{\varepsilon}_{z1}^{T}$ =10^{-3} s^{-1}) and a true axial strain-rate close to the transition strain-rate $\dot{\varepsilon}_t$ as the second point (e.g. $\dot{\varepsilon}_{z2}^{T}$ =10 s^{-1}) to determine K_6 based on the experimental data reported in Richeton et al.(2006). In case when extra experimental data between $\dot{\varepsilon}_{z1}^{T}$ and $\dot{\varepsilon}_t$ are available, K_6 may be determined by

$$K_6 = \frac{\sum_{j=1}^{I} K_6^j}{I}, \tag{10}$$

in which $K_6^j = \frac{\lg\left(\sigma_{dy2}^j / \sigma_{dy1}\right)}{\lg\left(\dot{\varepsilon}_{z2}^{Tj} / \dot{\varepsilon}_{z1}^{T}\right)}$ with $\left(\sigma_{dy2}^j, \dot{\varepsilon}_{z2}^{Tj}\right)$(j$\in I$) being the jth pair of I pairs of experimental data in the strain-rate range of $\dot{\varepsilon}_{z1}^{T} \le \dot{\varepsilon}_{z}^{T} \le \dot{\varepsilon}_t$.

It is stated by Walley et al.(1989) that rough estimation of the strain-rate dependence can be calculated by using the low- and medium-strain-rate data. An approximate strain-rate dependence value is estimated to be 4.86 MPa per decade of strain-rate for the investigated PC material based on the experimental data in Richeton et al.(2006) at strain-rates between 10^{-3} and 10 s^{-1}, which is very close to the values given by Walley et al.(1989) [i.e. 5.0 MPa per decade of strain-rate for PC, see Tab.7 in Walley et al.(1989)], and also close to those estimated from Rietsch and Bouette(1990) and Dioh et al.(1993) [i.e. 3.04 MPa and 4.01 MPa per decade of strain-rate for PC based on Fig.2 in Rietsch and Bouette(1990) and Fig.5 in Dioh et al.(1993), respectively]. These estimations did not consider the possible influence of confinement effect, which is observed in Fig.9 even before the transition strain-rate. We used Fig.9 to correct experimental results and the corrected strain-rate dependence is reduced to 3.43 MPa per decade of strain-rate between 10^{-3} and 10 s^{-1}. This value and Eq.(9) determine K_6=0.0178, which defines the strain-rate dependence in Eq.(5), as shown later in Fig.11.

Details of the calibration procedure for the determination of other material coefficients

can be found in Duan et al.(2001). Coefficients of $K_0 \sim K_7$ determined for the PC under investigation are all based on the test results in Richeton et al.(2006), which are summarized in Tab.2.

Tab.2 Material coefficients in Eq.(5) for PC

Material	K_0 (MPa)	K_1	K_2	K_3	K_4	K_5	K_6	K_7
PC	28.40	-4.1	615.91	22.40	69.83	6.80	0.0178	1.52

Tab.3 Constants $P_1 \sim P_4$ for PC

Material	P_1	P_2	P_3	P_4
PC	0.776	0.114	0.029	0.224

For the strain-rate range studied in this paper, it is reasonable to assume that the deformation process is essentially adiabatic. The governing equation for the increase of temperature, ΔT , at each increment of plastic strain is

$$\Delta T = \eta \frac{(\bar{\sigma}^{old} + \bar{\sigma}^{new})\Delta\bar{\varepsilon}}{2\rho h}, \qquad (11)$$

where ρ is the material density; h is the specific heat, which is not given in Richeton et al.(2006), is taken to be 1172 $\mathrm{J \cdot kg^{-1} \cdot K^{-1}}$ for the PC under investigation according to Siviour et al.(2005) who used similar grade of PC in SHPB tests; $\bar{\sigma}^{old}$ is the equivalent stress at the beginning of a plastic strain increment; $\bar{\sigma}^{new}$ is the equivalent stress at the end of the plastic strain increment; $\Delta\bar{\varepsilon}$ is the increment of equivalent plastic strain; η is the fraction of dissipated plastic energy which converts into thermal energy. It has been shown in Li and Lambros(2001) that the integral form of η decreases with strain in a small range, and then, reaches a plateau at a value of 0.5 when the strain is greater than the yield strain, which implies that a constant value of 0.5 can be used for the plastic response of PC. When η is a constant, its differential form is the same as its integral form [Li and Lambros(2001)].

Therefore, η =0.5 is used in Eq.(11) in the present study.

In order to consider the effect of interface friction between pressure bars and the specimen on the SHPB results, the kinetic friction model fitted by an exponential-linear function [Li et al.(2009)] is used for easy implementation into numerical simulations, i.e.

$$\mu_d / \mu_s = P_1 \exp(-V / P_2) + P_3 V + P_4 . \quad (12)$$

in which μ_d and μ_s are the kinetic and static friction coefficient, respectively; V is the maximum relative radial velocity, and μ_d / μ_s =1 when V =0; $P_1 \sim P_4$ are constants obtained from the test results between μ_d / μ_s and V . Values of $P_1 \sim P_4$ in Tab.3 are determined from kinetic friction tests between PC and steel in Meng(2002).

The equivalent flow stress $\bar{\sigma}$ decreases with the increase of temperature according to Eq.(5), which gives a framework to account for the thermo-mechanical coupling during high strain-rate plastic deformation. An algorithm of elastic-prediction-plastic-correction is applied to update the stress tensor of each material point where the first predicted stress tensor is based on generalized Hooke's law and the input values of elastic modulus and Poisson's ratio. At the end of each plastic strain increment, the predicted stress tensor is corrected using Eq.(5). Equation (11) is applied to calculate the increase of the local temperature of the polymer. Equation (12) is employed to implement the interface friction effect into ABAQUS using user subroutine VFRIC. Based on the above framework, an ABAQUS user material subroutine VUMAT was encoded and applied in the finite element simulations to implement the constitutive model Eq.(5), the thermomechanical coupling model and the kinetic friction model.

4. Results and Discussion

In order to validate the numerical model in Section 3, numerical SHPB tests (Fig.3) are performed on PC specimens tested by Richeton et al.(2006) in high strain-rate compression SHPB tests. The SHPB specimen has dimensions of 3.18 mm in thickness and 6.35 mm in

diameter. The kinetic friction model described by Eq.(12) is applied in the numerical SHPB simulations to model the friction effect between the interfaces of pressure bars and the specimen. Richeton et al.(2006) used SHPB tests to obtain true axial stress–strain curves of PC at true axial strain-rates of 600, 2100 and 3000 s^{-1} without giving the associated striking velocities. We have to adjust striking velocities in our numerical SHPB model to achieve these true axial strain-rates at yielding point, which are determined as 4.0, 9.3 and 12.4 m/s, respectively. True axial stress–strain curves of PC under these true axial strain-rates based on numerical SHPB tests are compared with corresponding experimental results from Richeton et al.(2006) in Fig.10. Very good agreement between modeling and experimental results on true axial stress–strain curve is demonstrated to validate the model, which will be used to study the dependence of DIF with the true axial strain-rate in SHPB tests.

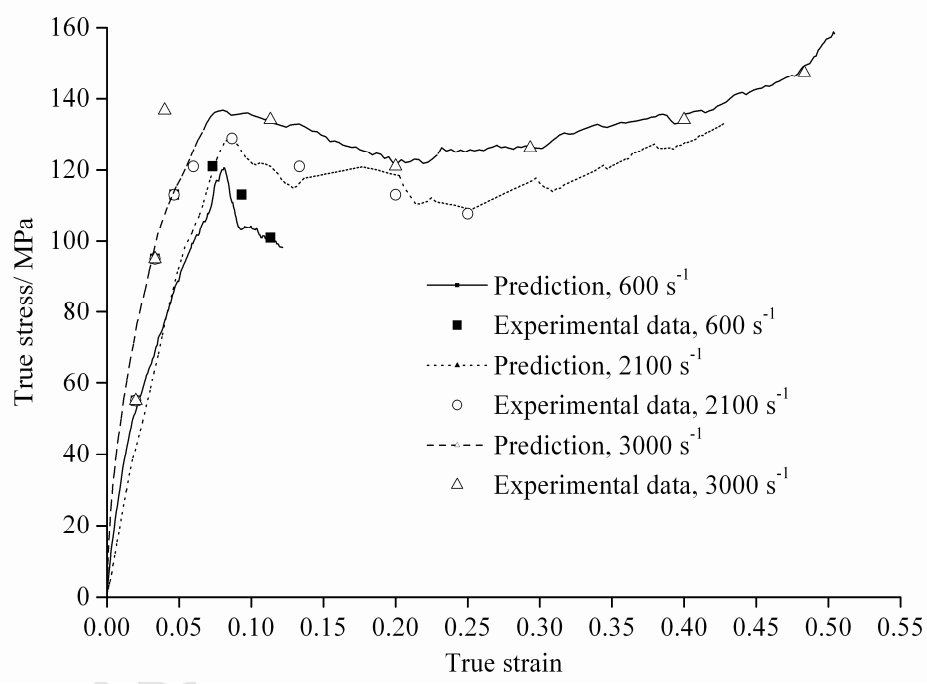

Fig.10. Numerical and experimental true axial stress–strain curves in compression for PC specimens under various true axial strain-rates [experimental data are taken from Richeton et al.(2006)].

Figure 11 shows the variations of DIF with logarithm true axial strain-rate from SHPB tests and numerical SHPB simulations for PC specimens that have a slenderness ratio of 0.5 and diameter of 6.35 mm, where the input DIF curve as described in Section 3 is also shown. Similar to the observations reported in Section 2.4, it is found that the dependence of apparent DIF on logarithm true axial strain-rate is insensitive to slenderness ratio in the numerical SHPB tests based on the dynamic constitutive model. The numerical SHPB model gives very good predictions on the variation of DIF with logarithm true axial strain-rate of PC reported in various independent SHPB tests, which implies that the dynamic stress enhancement of polymers is due to combined effects of the real strain-rate, temperature, lateral confinement, and interface friction, rather than pure strain-rate effect.

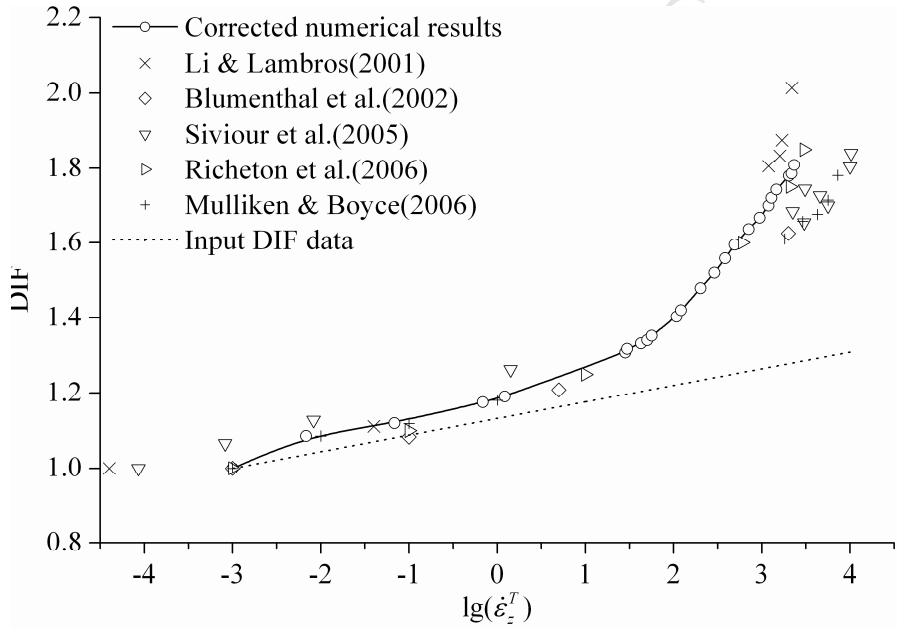

Fig.11. Comparison between the measured DIF from SHPB tests and finite element predicted DIF where hydrostatic pressure, strain-rate, thermal and friction effects are implemented for PC specimens.

According to our computations, it is found that the methodology proposed in this study can be applied to study the observed strain-rate enhancement of other polymers, e.g. PMMA and

high density polyethylene (HDPE), based on SHPB tests, although material parameters for them are different from those of PC.

5. Conclusions

Numerical SHPB tests show that the radial inertia stress developed in polymeric material specimens in SHPB tests and the interface friction between pressure bars and the polymer sample produce lateral confinement, which causes an apparent increase of the DIF of polymers. This effect becomes significant when the true axial strain-rate is beyond the transition strain-rate between 10^1~10^2 s^{-1}, coinciding with the experimentally observed transition strain-rate from a weak strain-rate-dependency to a strong strain-rate-dependency. The observed strain-rate dependence beyond this transition strain-rate in SHPB tests on polymers contains combined effects of real strain-rate, lateral confinement, thermal softening and interface friction. Misinterpretation of such combined effects as only strain-rate effect in design and numerical models may give inaccurate predictions of dynamic yield stress for polymers. Since the DIF for the description of strain-rate dependence is a non-dimensional parameter, it is expected that the conclusions obtained for the examined PC examples may be extended to other similar polymers although further works are necessary to confirm this.

Acknowledgements: First author acknowledges the scholarship from the School of Mechanical, Aerospace and Civil Engineering, The University of Manchester and the financial support from Henry Lester Trust.

References

ABAQUS Theory Manual, version 6.7-1. Hibbitt, Karlson & Sorensen, Inc, 2007.

Arriaga A, Lazkano JM, Pagaldai R, Zaldua AM, Hernandez R, Atxurra R, Chrysostomou A. Finite-element analysis of quasi-static characterization tests in thermoplastic materials: Experimental and numerical analysis results correlation with ANSYS. Polym Test

2007;26:284-305.
Bardia P, Narasimhan R. Characterization of pressure-sensitive yielding in polymers. Strain 2006;42:187-196.
Benaceur I, Othman R, Guegan P, Dhieb A, Damek F. Sensitivity of the flow stress of Nylon 6 and Nylon 66 to strain-rate. Int J Modern Phys B 2008;22:1249-1254.
Bertholf LD, Karnes CH. Two dimensional analysis of the split Hopkinson pressure bar system. J Mech Phys Solids 1975;23:1-19.
Blumenthal WR, Cady CM, Lopez MF, Gray GTIII, Idar DJ. Influence of temperature and strain rate on the compressive behavior of PMMA and polycarbonate polymers. AIP Conf Proc 2002:665-668.
Bowden PB, Jukes JA. The plastic flow of isotropic polymers. J Mater Sci 1972;7:52-63.
Bowden FP, Tabor D. Friction: an introduction to tribology. Anchor/Doubleday 1973, New York.
Brady TE, Yeh GSY. Yielding behavior of glassy amorphous polymers. J Appl Phys 1971;42: 4622-4630.
Briscoe BJ, Nosker RW. The influence of interfacial friction on the deformation of high density polyethylene in a split Hopkinson pressure bar. Wear 1984;95:241-262.
Briscoe BJ, Nosker RW. Flow stress of high density polyethylene at high rates of strain. Polym Commun 1985;26:307-308.
Carapellucci L, Yee A. The biaxial deformation and yield behavior of bisphenol-a polycarbonate: effect of anisotropy. Polym Eng Sci 1986;26:920-930.
Chen WN, Lu F, Cheng M. Tension and compression tests of two polymers under quasi-static and dynamic loading. Polym Test 2002;21:113-121.
Chen WN, Luo H. Dynamic compressive responses of intact and damaged ceramics from a single split Hopkinson pressure bar experiment. Exp Mech 2004;44:295-299.
Chen WN, Zhang X. Dynamic response of Epon 828/T-403 under multiaxial loading at various temperatures. ASME J Eng Mater Tech 1997;119:305-308.
Chou SC, Robertson KD, Rainey JH. The effect of strain rate and heat developed during deformation on the stress-strain curve of plastics. Exp Mech 1973;13:422-432.
Chowdhury KA, Benzerga AA, Talreja R. A computational framework for analyzing the dynamic response of glassy polymers. Comput Methods Appl Mech Eng 2008;197:4485-

4502.
Chowdhury SR, Narasimhan R. A finite element analysis of stationary crack tip fields in a pressure sensitive constrained ductile layer. Int J Solids Struct 2000;37:3079-3100.
Davies EDH, Hunter SC. The dynamic compression testing of solids by the method of the split Hopkinson bar. J Mech Phys Solids 1963;11:155-179.
Dioh NN, Leevers PS, Williams JG. Thickness effects in split Hopkinson pressure bar tests. Polym 1993;34:4230-4234.
Dioh NN, Ivankovic A, Leevers PS, Williams JG. Stress wave propagation effects in split Hopkinson pressure bar tests. Proc R Soc London A 1995;499:187-204.
Duan Y, Saigal A, Greif R, Zimmerman MA. A uniform phenomenological constitutive model for glassy and semicrystalline polymers. Polym Eng Sci 2001;41:1322-1328.
Duan Y, Saigal A, Greif R, Zimmerman RA. Impact behavior and modeling of engineering polymers. Polym Eng Sci 2003;43:112-124.
Eyring H. Viscosity, plasticity and diffusion as examples of absolute reaction rates. J Chem Phys 1936;4:283-291.
Field JE, Walley SM, Proud WG, Goldrein HT, Siviour CR. Review of experimental techniques for high rate deformation and shock studies. Int J Impact Eng 2004;30:725-775.
Frew DJ, Forrestal MJ, Chen W. Pulse shaping techniques for testing elastic-plastic materials with a split Hopkinson pressure bar. Exp Mech 2005;45:186-195.
Gary G, Bailly P. Behaviour of quasi-brittle material at high strain rate, experiment and modeling. Eur J Mech A 1998;17:403-420.
Gavrus A, Le Baron J.-P., Caestecker P, Ragneau E. Investigation of high speed behaviour of ductile materials by computer simulation and Hopkinson experimental test. Advances in Mechanical Behaviour, Plasticity and Damage, Tours, November 2000, 535-540.
Gavrus A, Caestecker P, Ragneau E, Davoodi B. Analysis of the dynamic SHPB test using the finite element simulation. J Phys IV France 2003;110:353-358.
Gorham DA, Pope PH, Cox O. Sources of error in very high strain rate compression tests. Inst Phys Conf Ser 1984;70:151-158.
Gorham DA. Specimen inertia in high strain-rate compression. J Phys D: Appl Phys. 1989;22:1888-1893.
Gorham DA. An effect of specimen size in the high strain rate compression test. J Phys IV

1991;C3:411-418.
Gorham DA, Pope PH, Field JE. An improved method for compressive stress-strain measurements at very high strain rates. Proc R Soc Lond A 1992;438:153-170.

Gray GT. Classic split-Hopkinson pressure bar testing. ASM Handbook, Mechanical Testing and Evaluation, Materials Park, OH, 2000;8:462-476.

Grote DL, Park SW, Zhou M. Dynamic behaviour of concrete at high strain rates and pressure: I. Experimental characterization. Int J Impact Eng 2001;25:869-886.

Haddow JB. On compression of thin disk. Int J Mech Sci 1965;7:657-660.

Hall IW, Guden M. Split Hopkinson pressure bar compression testing of an aluminum alloy: effect of lubricant type. J Mat Sci Letters 2003;22:1533-1535.

Hartley RS, Cloete TJ, Nurick GN. An experimental assessment of friction effects in the split Hopkinson pressure bar using the ring compression test. Int J Impact Eng 2007;34: 1705-1728.

Hasegawa T, Okazaki K. Analysis of strain rate dependence of tensile elongation for a mechanical milling Al-1.1Mg-1.2Cu alloy tested at 748 K from a dislocation dynamics viewpoint. Mater Sci Eng A 1999;260:294-300.

Haufe A, Bois PD, Kolling S, Feucht M. A semi-analytical model for polymers subjected to high strain rates. Fifth European LS-Dyna users conference, 2005.

Kolsky H. An investigation of the mechanical properties of materials at very high rates of loading. Proc Phys Soc London B 1949;62:676-700.

Lee OS, Kim GH. Thickness effect on the mechanical behavior of a composite material (1001P) and polycarbonate in split Hopkinson pressure bar technique. J Mater Sci Letters 2000;19:1805-1808.

Li QM, Meng H. About the dynamic strength enhancement of concrete-like materials in a split Hopkinson pressure bar test. Int J Solids Struct 2003;40:343-360.

Li QM, Lu YB, Meng H. Further investigation on the dynamic compressive strength enhancement of concrete-like materials based on split Hopkinson pressure bar tests, Part II: numerical simulations. Int J Impact Eng 2009;36:1335-1345.

Li ZH, Lambros J. Strain rate effects on the thermomechanical behavior of polymers. Int J Solids Struct 2001;38:3549-3562.

LIGO note. Blade process specification. http://www.ligo.caltech.edu/, LIGO-T040108-00-K, 2005.

Lindholm US. Some experiments with split Hopkinson pressure bar. J Mech Phys Solids 1964;12:317-335.

Malinowski JZ, Klepaczko JR. A unified analytic and numerical approach to specimen behaviour in the split-Hopkinson pressure bar. Int J Mech Sci 1986;28:381-391.

Meng H. Numerical split Hopkinson pressure bar (NSHPB) test and its applications in the assessment and improvement of SHPB test results. PhD dissertation, Nanyang Technological University, Singapore, 2002.

Meng H, Li QM. Correlation between the accuracy of a SHPB test and the stress uniformity based on numerical experiments. Int J Impact Eng 2003;28:537-555.

Mulliken AD, Boyce MC. Mechanics of the rate-dependent elastic-plastic deformation of glassy polymers from low to high strain rates. Int J Solids Struct 2006;43:1331-1356.

Pampillo CA, Davis LA. Volume change during deformation and pressure dependence of yield stress. J Appl Phys 1971;42:4674-4679.

Quinson R, Perez J, Rink M, Pavan A. Yield criteria for amorphous glassy polymers. J Mater Sci 1997;32:1371-1379.

Raghava R, Caddell R, Yeh G.. The macroscopic yield behaviour of polymers. J Mater Sci Lett 1973;8:225-232.

Richeton J, Ahzi S, Vecchio KS, Jiang FC, Adharapurapu, RR. Influence of temperature and strain rate on the mechanical behavior of three amorphous polymers: characterization and modeling of the compressive yield stress. Int J Solids Struct 2006;43:2318-2335.

Rietsch F, Bouette B. The compression yield behaviour of polycarbonate over a wide range of strain rates and temperatures. Eur Polym J 1990;26:1071-1075.

Rittel D, Brill A. Dynamic flow and failure of confined polymethylmethacylate. J Mech Phys Solids 2008;56:1401-1416.

Rittel D, Dorogoy A. A methodology to assess the rate and pressure sensitivity of polymers over a wide range of strain rates. J Mech Phys Solids 2008:56:3191-3205.

Samanta SK. Dynamic deformation of aluminium and copper at elevated temperature. J Mech Phys Solids 1971;19:117-122.

Siviour CR, Walley SM, Proud WG, Field JE. The high strain rate compressive behavior of

polycarbonate and polyvinylidene difluoride. Polym 2005;46:12546-12555.

Song L, Hu SS. Two-wave and three-wave method in SHPB data processing. Explosion Shock Waves 2005;25:368-373 (in Chinese).

Trautmann A, Siviour CR, Walley SM, Field JE. Lubrication of polycarbonate at cryogenic temperatures in the split Hopkinson pressure bar. Int J Impact Eng 2005;31:523-544.

Walley SM, Field JE, Pope PH, Safford NA. A study of the rapid deformation behavior of a range of polymers. Phil Trans R Soc Lond A 1989;328:1-33.

Wang TT, Zupko HM, Wyndon LA, Matsuoka S. Dimensional and volumetric changes in cylindrical rods of polymers subjected to a twist moment. Polym 1982;23:1407-1409.

Yin ZN, Wang TJ. Deformation of PC/ABS alloys at elevated temperatures and high strain rates. Mater Sci Eng A 2008;494:304-313.

Young RJ, Lovell PA. Introduction to polymers (2ed edition). CRC Press, 1991, pp.366.

Zencker U, Clos R. Limiting conditions for compression testing of flat specimens in the split Hopkinson pressure bar. Exp Mech 1999;39:343-348.

Zhang M, Wu HJ, Li QM, Huang FL. Further investigation on the dynamic compressive strength enhancement of concrete-like materials based on split Hopkinson pressure bar tests Part I: Experiments. Int J Impact Eng 2009;36:1327-1334.

Zhao H. Study of specimen thickness effects in the impact tests on polymers by numeric simulations. Polym 1998;39:1103-1106.